Title

Gene location and DNA density determine transcription factor distributions in Escherichia coli

Journal

Molecular Systems Biology, 8(1)

ISSN

1744-4292

Authors

Kuhlman, Thomas E
Cox, Edward C

Publication Date

2012

DOI

10.1038/msb.2012.42

Peer reviewed

Molecular Systems Biology 8; Article number 610; doi:10.1038/msb.2012.42
Citation: ***Molecular Systems Biology*** **8:610**

www.molecularsystemsbiology.com

molecular systems biology

Gene location and DNA density determine transcription factor distributions in *Escherichia coli*

Thomas E Kuhlman[1,2,*] and Edward C Cox[1]

[1] Department of Molecular Biology, Princeton University, Princeton, NJ, USA and [2] Department of Physics, University of Illinois at Urbana-Champaign, Urbana, IL, USA
* Corresponding author. Department of Physics, University of Illinois at Urbana-Champaign, 1110 West Green Street, Urbana, IL 61801, USA. Tel.: +1 858 531 4386; Fax: +1 217 244 7187; E-mail: tkuhlman@illinois.edu

Received 16.3.12; accepted 9.8.12

The diffusion coefficient of the transcription factor LacI within living *Escherichia coli* has been measured directly by *in vivo* tracking to be $D = 0.4\,\mu m^2/s$. At this rate, simple models of diffusion lead to the expectation that LacI and other proteins will rapidly homogenize throughout the cell. Here, we test this expectation of spatial homogeneity by single-molecule visualization of LacI molecules non-specifically bound to DNA in fixed cells. Contrary to expectation, we find that the distribution depends on the spatial location of its encoding gene. We demonstrate that the spatial distribution of LacI is also determined by the local state of DNA compaction, and that *E. coli* can dynamically redistribute proteins by modifying the state of its nucleoid. Finally, we show that LacI inhomogeneity increases the strength with which targets located proximally to the LacI gene are regulated. We propose a model for intranucleoid diffusion that can reconcile these results with previous measurements of LacI diffusion, and we discuss the implications of these findings for gene regulation in bacteria and eukaryotes.
Molecular Systems Biology **8**: 610; published online 11 September 2012; doi:10.1038/msb.2012.42
Subject Categories: chromatin & transcription; microbiology & pathogens
Keywords: facilitated diffusion; genome organization; single molecule microscopy; transcriptional regulation

Introduction

Regulation of gene expression by the binding and unbinding of transcription factor proteins (TFs) at specific regulatory sites in response to environmental stimuli is the fundamental mechanism organisms use to adapt to changing environments. An understanding of how TFs search for and find their binding targets is thus of fundamental importance if we are to understand the design and behavior of genetic circuits and their components (Gerland *et al*, 2002). The seminal theoretical and *in vitro* work of Berg, Winter, and von Hippel forms the basis for our current understanding of the TF search mechanism known as facilitated diffusion: TFs are thought to bind non-specifically and slide in one dimension along the DNA, in addition to three-dimensional diffusion throughout the cytoplasm (Berg *et al*, 1981; Winter and von Hippel, 1981; Winter *et al*, 1981). Recent studies of the *lac* repressor, perhaps the best-studied transcription factor in *E. coli*, have revealed that diffusion of repressor in live cells is rapid, of order $D \sim 0.4\,\mu m^2/s$ (Elf *et al*, 2007). At this rate, a single molecule travels the length of *E. coli* in 1–10 s, and simple models reveal that the distribution of repressor should be homogeneous throughout the DNA and cell.

Here, we test this expectation by using high-throughput single-molecule microscopy to determine the average spatial distribution of *lac* repressor, LacI, in a strain deleted for the native *lac* operon. Because these strains lack a specific binding target, we can ask if the theoretical expectation of uniform distribution along the DNA and in the cytoplasm is met. Surprisingly, we find that the distribution is inhomogeneous and dependent on the location of the repressor gene, showing that our current understanding of the search process is far from complete. We further show that this inhomogeneity is the result of competition between non-specific DNA binding on the one hand and exclusion of the repressor from DNA on the other hand. Finally, we show that this inhomogeneity can be detected as stronger repression of targets located near the TF gene than would be expected from a homogenous repressor distribution, and we discuss the implications of these findings for gene regulation and the evolution of genome organization.

Results

To visualize the spatial distribution of non-specifically bound *lac* repressor molecules, we integrated a gene encoding LacI fused to the fluorescent reporter Venus at four different chromosomal locations in a strain where all *lac* repressor binding sites have been deleted (Kuhlman and Cox, 2010). These sites were near the replication origin of the circular genome, near the replication terminus, or halfway between the origin and terminus on the right or left halves of the chromosome, or replichores (Supplementary Figure 1A), and particular care was taken not to include any pseudooperators

overlapping the 3′ end of either *lacI* or *venus* (Oehler *et al*, 1990, 1994; Müller-Hill, 1998; Elf *et al*, 2007). These strains were grown to exponential steady state (Supplementary Figure 2), fixed with paraformaldehyde, and imaged to determine the spatial distribution of non-specifically bound LacI-Venus molecules using total internal reflection fluorescent (TIRF) microscopy, the distribution of DNA using staining with 4′,6-diamidino-2-phenylindole (DAPI), the location of the *lacI-venus* integration sites determined by the fluorescent reporter-operator system (FROS; Joshi *et al*, 2011), and the corresponding *lacI-venus* mRNA distributions determined by fluorescence *in situ* hybridization (FISH; Raj *et al*, 2008; So *et al*, 2011).

We took ~1000 images for each strain and growth condition. We then used an automated cell-finding algorithm to identify individual cells in each image, binned cells by size, and averaged the fluorescent intensity at each pixel to determine the average spatial distribution of each component (Figure 1). Due to hardware limitations, we were unable to dynamically switch between epifluorescent and TIRF illumination, and this limitation precludes the simultaneous high-throughput measurement and direct correlation of gene location and protein distribution in the same cell. Consequently, imaging of the spatial distribution of each component (DNA, gene, mRNA, and protein) was performed in separate measurements. The absolute orientation of each cell is then ambiguous, and we additionally perform an average over all possible orientations, which introduces symmetries into the resulting average distributions.

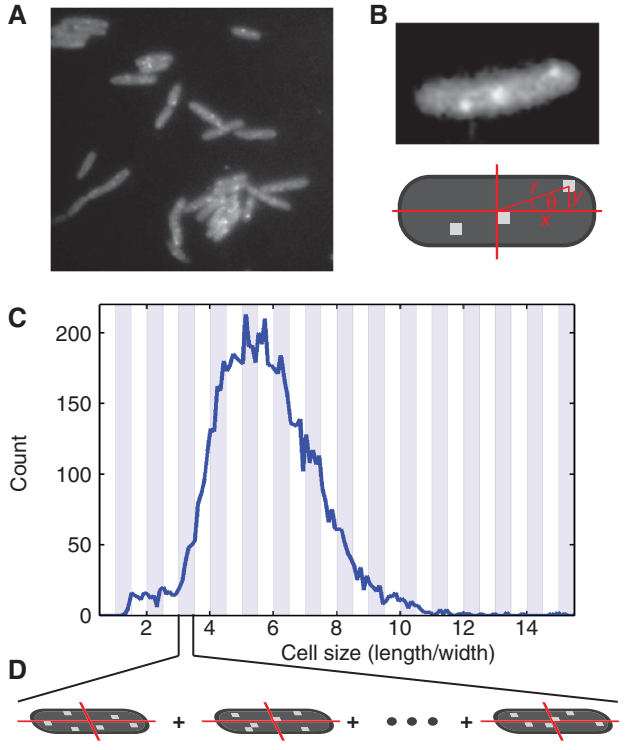

Figure 1 Image averaging procedure. (**A**) A representative image field with *lacI-venus* integrated near the origin (*atpI* locus) imaged at × 133 magnification. (**B**) Individual cells are found using an automated algorithm, and coordinates are established at the cellular centroid to measure cellular dimensions and the location of each pixel. (**C**) Because of the narrow distribution of cell widths, correctly identified cells are identified according to correspondence with the appropriate width and binned according to the ratio of the length to width. Alternating gray and white bars indicate each bin. (**D**) Cells within each bin are rescaled to the size of the average cell within that bin and averaged together on a per-pixel basis and over all orientations.

Repressor gene location influences TF distributions

The average distributions of DNA, *lacI-venus* gene location, *lacI-venus* mRNA, and LacI-Venus protein for cells that have just divided are shown in Figure 2. We find that the replication origin-proximal integration locus is located midcell and the terminus-proximal locus at a superposition of the poles and midcell (Bates and Kleckner, 2005; Wiggins *et al*, 2010). These results are in broad agreement with the existing literature (Niki *et al*, 2000; Wang *et al*, 2006; Montero Llopis *et al*, 2010; Wiggins *et al*, 2010). FISH reveals *lacI* mRNA to be localized at the gene loci for origin and terminus integrants (Montero Llopis *et al*, 2010). When the *lacI* source gene is located on a medium copy number plasmid localized to the poles (Figure 2, second column), *lacI-venus* RNA shows some tendency to redistribute to other locations in the cell and LacI-Venus is evenly distributed throughout the nucleoid. When the source is located within the chromosome, however, we find that the distributions depend on the position of the encoding gene on the chromosome, and correlate with the spatial distributions of the source genes.

Recalling that these strains are deleted for specific LacI binding targets, interpretation of the LacI-Venus distributions for origin and terminus integrants is straightforward: when the source is near the origin, the gene, mRNA, and protein map to that location. When the source gene is integrated at the terminus, the average gene location shifts toward the poles, and the LacI distribution changes correspondingly. Furthermore, the LacI-Venus molecular phenotypes depend on the LacI DNA binding domain. LacI-Venus strains with insertions at the same locations but deleted for first 42 base pairs of the *lacI* coding sequence (the 14 amino acid residues of the DNA binding domain; henceforth referred to as LacI42-Venus) show that, in the absence of the DNA binding domain, the LacI-Venus distributions at the origin and terminus alter dramatically (Figure 2, last row).

DNA density affects TF distributions

E. coli changes its morphology and the gross compaction state of its nucleoid in response to changing growth conditions. We assayed the spatial distribution of LacI-Venus in a variety of growth states to determine whether these changes in the intracellular environment affect the steady-state distribution of LacI-Venus protein. The results for cells containing an equal total amount of DNA in different growth states are shown in Figures 3 and 4. When bulk growth is arrested in stationary phase cells generally contain a single chromosome, are morphologically small, and the DNA is densely packed (Figure 3, second column; Supplementary Figure 3). As the growth rate increases, cells become larger and the DNA becomes more loosely packed (Figure 3, third column; Supplementary

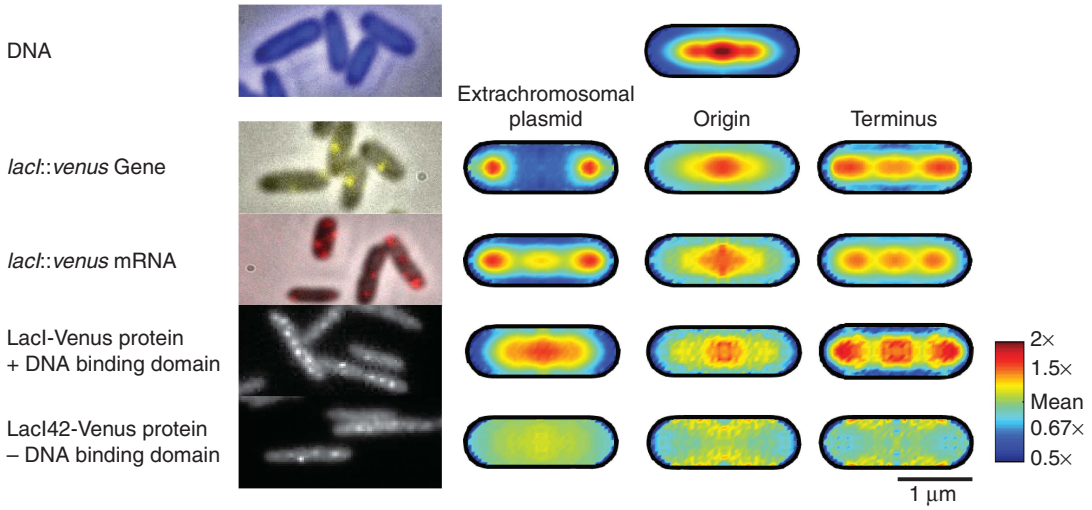

Figure 2 Average spatial distribution of *lacI-venus* expression. Cells were grown in M63 minimal medium + 0.5% glycerol before fixation. Averages are for cells of 1.9–2.2 μm in length, the bin identified in Figure 1D. Averages are also taken over all cell orientations, resulting in the symmetry of each plot. Raw images of combined transmitted and fluorescence channels are shown in the first column for DNA (× 400, DAPI staining; row 1), gene locus (× 400, FROS; row 2), mRNA (× 400, FISH; row 3), LacI-Venus protein (× 400, TIRF microscopy, row 4), and LacI-Venus protein without DNA binding domain (× 400, TIRF microscopy, row 5). Representative LacI-Venus images are at × 133magnification for visual clarity. Remaining columns show average distributions for each component with the *lacI-venus* source gene expressed from the indicated location. Fluorescent intensity is normalized to the mean fluorescence within the cell. The quantitative color scale is for LacI-Venus only; other averages are qualitatively scaled for comparison. The *essQ* locus was the LacI-Venus source for terminus, but the gene location shown is for the adjacent *n*th terminal locus for clarity (Kuhlman and Cox, 2010); *essQ* localization is identical but less clear due to reduced binding at that locus.

Figure 3). As cells reach their maximum growth rate of ~20 min/doubling they contain at least two or more complete sister chromatids (Figure 4, third column; Supplementary Figure 3), and the trend of DNA decondensation in fast growing cells continues compared with slower growing cells late in the life cycle which also contain two complete sister chromatids (Figure 4, second column).

It is possible that the more diffuse distribution of DNA in fast growing cells shown in Figure 4 is an artifact of image averaging: if the spatial positioning of condensed DNA within the larger volume of fast growing cells is highly variable, yet dense, averaging will make the resulting distribution appears less dense than each individual nucleoid. We therefore also quantified the compaction density of nucleoids in individual cells in each growth state by measuring the degree of geometric curvature of the DAPI fluorescent surface representing each nucleoid (see Supplementary information—Quantification of DNA Compaction). The results of this single-cell analysis are shown in Supplementary Figure 4, and demonstrate that the compaction density of DNA decreases monotonically as a function of growth rate when measured in individual cells.

Measurement of LacI-Venus distributions in each of these growth states reveals that the distributions are heavily dependent on the density of the DNA. When the DNA is most highly condensed in stationary phase, LacI42-Venus appears to be generally excluded from the DNA and localized toward the ends of the cell regardless of the source location. Conversely, the pattern of localization of LacI-Venus non-specifically bound to DNA correlates closely with the location of the source gene (Figure 3, compare first and second columns). Similarly, the distribution of LacI-Venus in exponentially slow growing cells containing a single chromosome also correlates closely with the distribution of its encoding gene (Figure 3, compare first and third columns). However, LacI42-Venus is no longer highly localized toward the ends of the cell and is instead more evenly distributed, although there is a weak general tendency to avoid the central nucleoid-occupied area of the cell. These subtle differences in distribution may be a consequence of different initial conditions due to different integration locations.

As the cells grow and replicate their DNA, the resulting sister chromatids segregate and gene loci move around within the cell. We show in Figure 4 the distribution of LacI-Venus in slow growing (left) and fast growing (right) cells containing two complete sister chromatids. We first notice the continued apparent tendency of LacI42-Venus to avoid the central spaces occupied by the nucleoid. For the slow growing midreplichore integrants, the intact LacI-Venus distributions correlate closely with the distribution of the corresponding gene. For the origin and terminus integrants, however, the correlation is less clear. Both distributions show hysteresis: i.e., the distribution of LacI-Venus in older cells depends upon the history of the location of the gene in younger cells, in the following sense: Before replication, the origin locus produces LacI-Venus at midcell. After replication and segregation, LacI-Venus pools in the inter-chromatid space near where the origin was originally, as judged by Figures 4 and 5. Similarly, after the terminus relocates to midcell after replication and segregation, there remains a pool of LacI-Venus further out toward the ends of the cell. We propose that this tendency of LacI-Venus to pool in the nearest available space that contains less DNA is also a result of a tendency toward nucleoid exclusion of LacI-Venus molecules, and may be related to previously observed asymmetry of the cell poles (Rang Camilla *et al*, 2011).

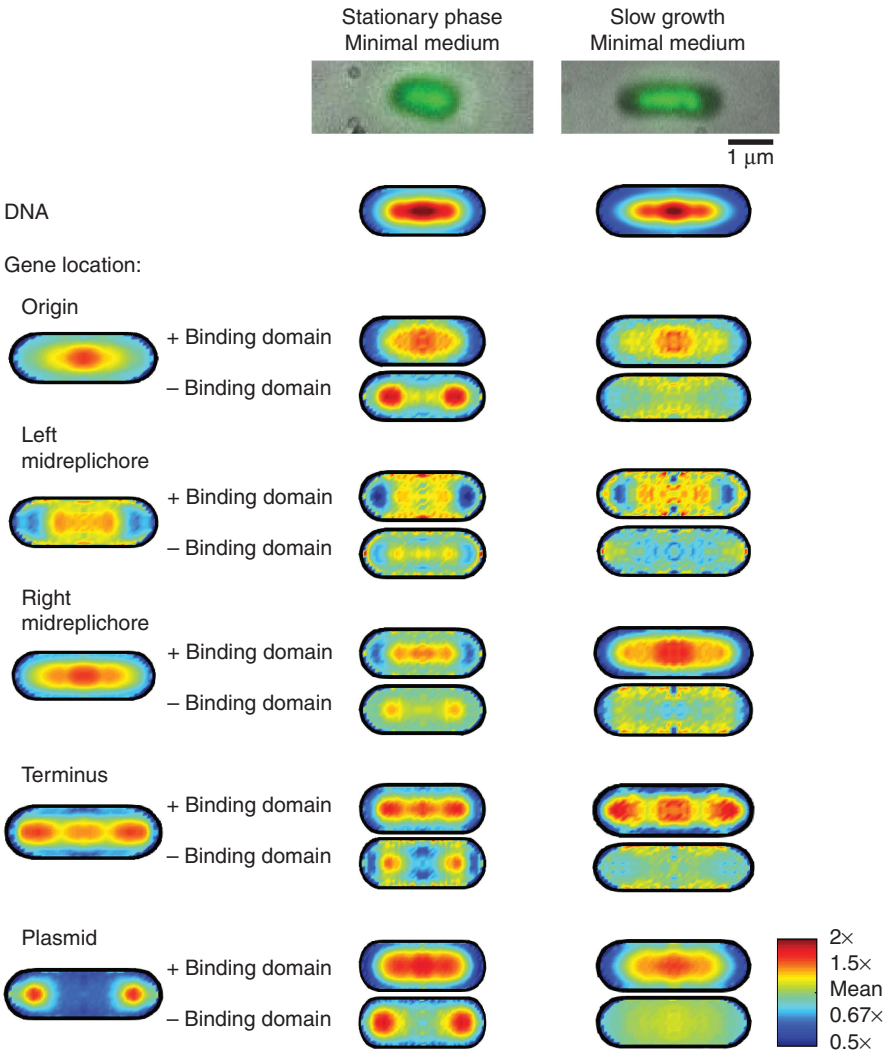

Figure 3 Average TF distributions as a function of growth state: one chromatid. Average DNA (first row) and LacI-Venus distributions with and without the DNA binding domain (subsequent groups of two rows, respectively) are shown as a function of *lacI-venus* gene integration location (rows) for stationary phase cells (left) and slow growing exponential phase cells containing one chromatid (right). Stationary phase results are from cells grown overnight in M63 minimal medium + 0.5% glycerol. LacI-Venus distributions were obtained by excitation with a 488-nm wavelength laser except in the case of the midreplichore integrants, where a 514-nm laser was used for excitation to increase the signal-to-noise ratio. The DAPI channel is shown as green in the first row to improve sensitivity to the eye. Average DNA content for exponential growth is scaled to be directly comparable to Figures 4 and 5 (see Supplementary Figure 3C and D and Kubitschek, 1974). Distributions of gene location in the first column are from cells grown in M63 + 0.5% glycerol that are 1.9–2.2 μm in length; gene distributions in stationary phase remain similar and are compared directly in Supplementary Figure 5A.

Finally, in fast growth conditions with less densely packed DNA the distributions of LacI-Venus do not obviously correlate with the distributions of the encoding genes, nor is it obvious that the LacI42-Venus shows any tendency toward nucleoid exclusion. Furthermore, the overall absolute correlation of the LacI-Venus distribution with the DNA distribution appears significantly weaker in the fast growth state than in the slow growth state. Compare, e.g., the correlation of the distribution of LacI-Venus with the DNA distributions when LacI-Venus is expressed at high levels from an extrachromosomal plasmid in the last row in Figure 4.

To further explore the influence of DNA density on the distribution of proteins, the compaction state of DNA can be manipulated directly by adding drugs that disrupt transcription and translation (Cabrera *et al*, 2009). Chloramphenicol binds to the ribosome and stops peptide synthesis, and also leads to the condensation of DNA. In Figure 5A, we show the change in average nucleoid density and the resulting redistribution of LacI-Venus in exponentially slow growing cells late in the life cycle after DNA replication following the addition of 200 μg/ml chloramphenicol; cross-sections through the longitudinal axis of the distributions at time $t = 0$ and $t = 10$ min are shown in Figure 5B, which show the expected bilobed nucleoid structure after chromosome replication and segregation. We quantify the amount of mass displacement at each time point, $D(t_i)$, by taking the difference

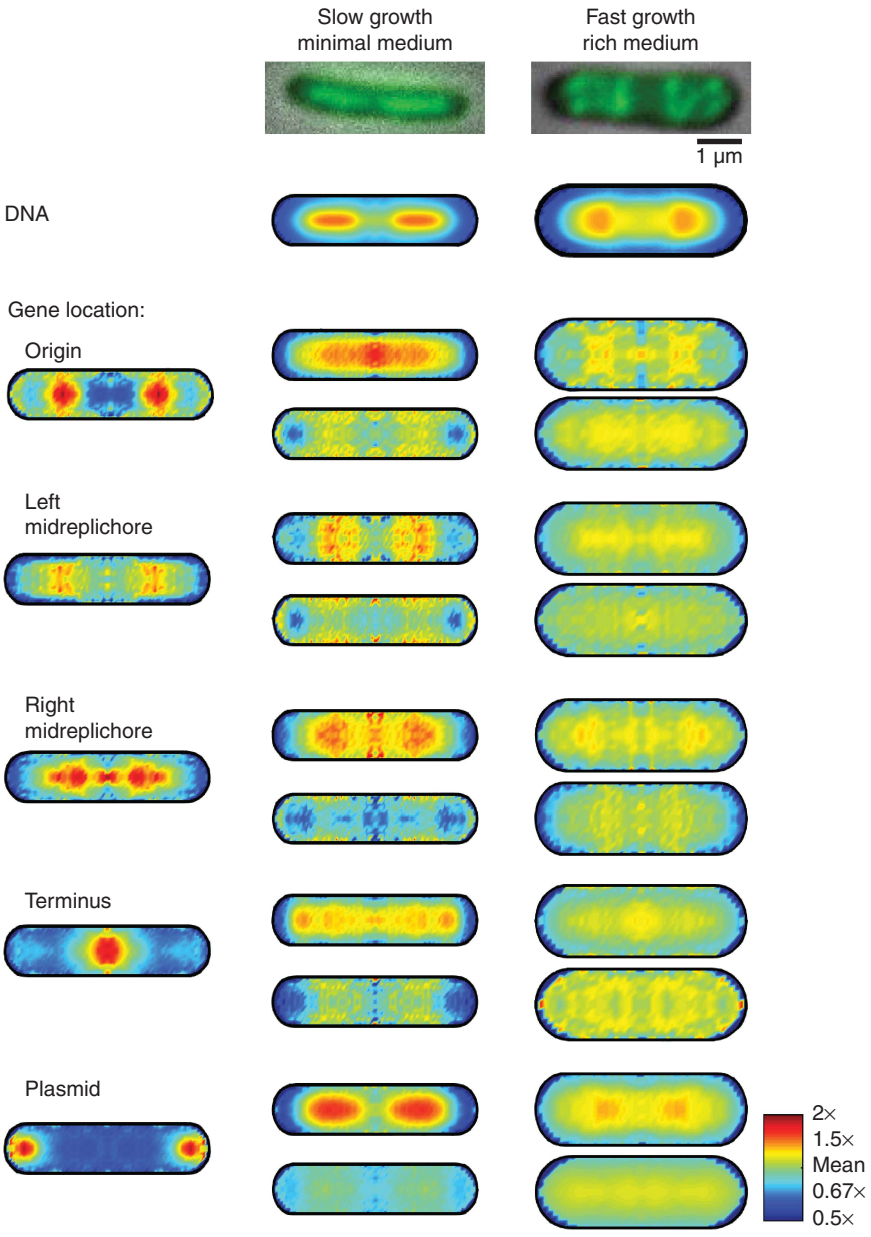

Figure 4 Average TF distributions as a function of growth state: two chromatids. Average DNA (first row) and LacI-Venus distributions with and without the DNA binding domain (subsequent groups of two rows, respectively) are shown as a function of *lacI-venus* gene integration location (rows) for exponentially slow growing cells in M63 + 0.5% glycerol (left) and exponentially fast growing cells containing two chromatids (right). Fast growth in RDM + 0.5% glucose yields a doubling time of 22 ± 2 min. Stationary phase results are from cells grown overnight in M63 minimal medium + 0.5% glycerol. LacI-Venus distributions of exponentially slow growing origin and terminus integrants we obtained by Venus excitation with a 488-nm wavelength laser; all other conditions were obtained with a 514-nm laser to increase the signal-to-noise ratio. Average DNA content in each case is scaled relative to slow growing cells containing one chromatid in Figure 4. Distributions of gene location shown in the first column are from growth in M63 + 0.5% glycerol that are 4.2–4.5 μm in length; gene distributions in exponential fast growth are similar and are compared directly in Supplementary Figure 5B.

between the initial distribution at time t_0, $F(x, y, t_0)$, and the distribution at each subsequent time point t_i, $F(x, y, t_i)$, according to

$$D(t_i) = \sum_{j,k} \left| F(x_j, y_k, t_i) - F(x_j, y_k, t_0) \right| \qquad (1)$$

The percentage of maximum displacement of both DNA (blue circles) and LacI-Venus (red circles) as a function of time is shown in Figure 5C, in which we simultaneously fit both data sets to a model assuming a constant rate of displacement β, i.e., $D(t) = 1 - e^{-\beta t}$. The simultaneous fit of both data sets to this model is shown as the black curve in Figure 5C, and we find a rate of mass displacement of $\beta = 0.60$/min. Since areas of high LacI-Venus density correspond inversely to areas of high DNA density after displacement, and the displacement of DNA and LacI-Venus occurs at comparable rates, the most

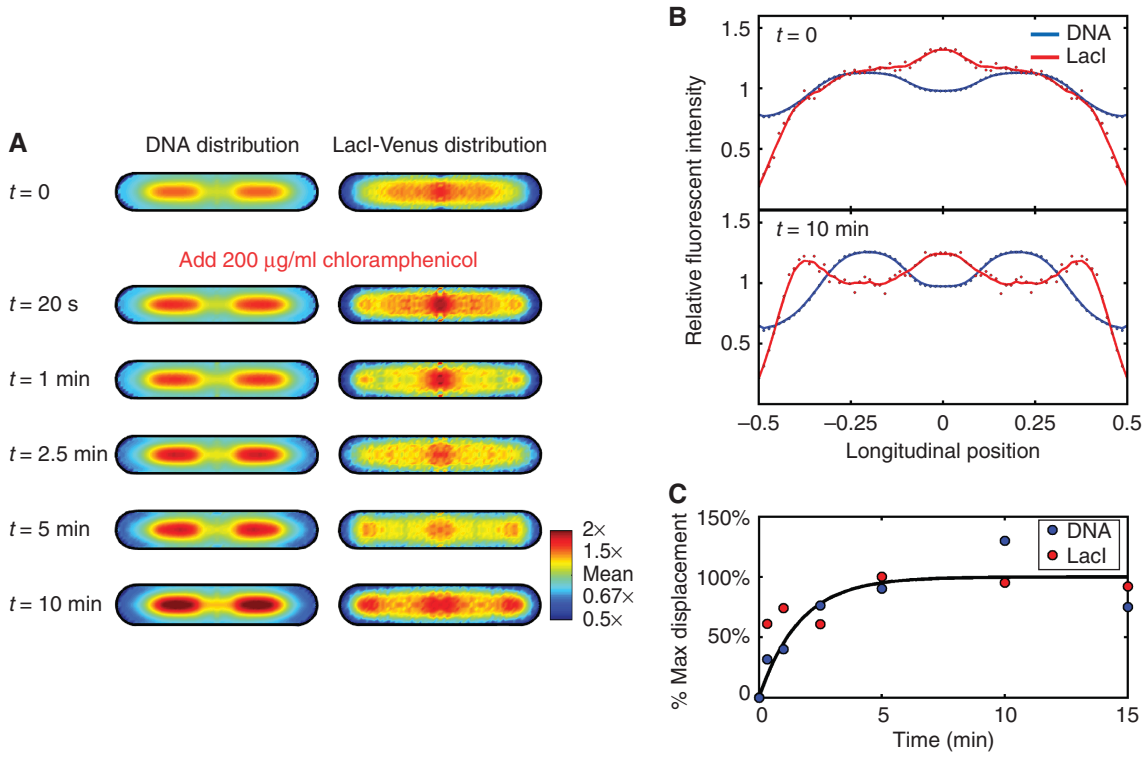

Figure 5 LacI redistribution as a result of nucleoid condensation. (**A**) The steady-state distribution of DNA and LacI-Venus in cells with *lacI-venus* integrated near the origin (*atpI* locus) and grown in M63 + 0.5% glycerol, cell length of 4.2–4.5 μm, are shown at $t = 0$. After this sample was taken, 200 μg/ml chloramphenicol was added directly to the culture and samples were withdrawn and fixed at the indicated times. Note that the color scale has been changed somewhat from Figure 4 to accommodate the condensed DNA. (**B**) Cross-sections along the longitudinal axis of the DNA (blue) and LacI-Venus (red) distributions at time $t = 0$ (top) and $t = 10$ min (bottom). Lines are a moving average of six adjacent points. (**C**) The rate of mass displacement. Displacement is quantified as the total difference between each distribution and the initial distribution at time $t = 0$. The black line corresponds to a simultaneous fit of both data sets to the equation $D(t) = 1 - e^{-\beta t}$. The equivalent result for LacI42-Venus is shown in Supplementary Figure 6. Source data is available for this figure in the Supplementary Information.

parsimonious explanation for these data is that the redistribution of LacI-Venus protein is driven by modifications of the DNA condensation state (see also Figures 3 and 4 and Supplementary Figure 6 for the equivalent result for LacI42-Venus and Supplementary Figure 7B for similar results showing a tendency for nucleoid exclusion in response to serine hydroxamate).

Nucleoid exclusion has previously been observed for large aggregates of proteins (Ebersbach *et al*, 2008; Winkler *et al*, 2010), and it is thought that exclusion may be driven by aggregation combined with entropic mechanisms (Saberi and Emberly, 2010). However, the distributions reported here are not due to LacI-Venus aggregation: expression levels from chromosomal sources are low (~1–10 molecules per cell; Gilbert and Muller-Hill, 1966), and bright spots in the images correspond to individual LacI-Venus dimers as judged by bleaching and blinking kinetics of fluorescent spots in individual fixed and living cells (Supplementary Figure 8). Furthermore, when a specific LacI binding target is present in the genome, LacI-Venus binds at the predicted location (Supplementary Figure 5D), the expected behavior for fully soluble and functional LacI dimers. The specific binding regions used in Supplementary Figure 5D are variants of the $P_{Llac\text{-}O1}$ promoter (Lutz and Bujard, 1997; Kuhlman and Cox, 2010). Since this promoter binds at most two dimers and is easily distinguished using our method, this is also a strong indication that we are imaging individual functional molecules.

The patterns of localization described here do not appear to be artifacts of fixation. We show in Supplementary Figure 7A images of live stationary phase cells expressing LacI42-Venus from both plasmid and chromosomal sources, showing the same pattern of localization toward the ends of the cells reported in Figure 3, and in Figure 5 in response to chloramphenicol. We also show in Supplementary Movie 1 a movie of those cells shown in Supplementary Figure 7A with a chromosomal LacI42-Venus source that shows that the motion of LacI42-Venus molecules is severely slowed and spatially localized toward the ends of the cell. The spots shown in this movie are single LacI42-Venus molecules as determined by blinking and bleaching kinetics (Supplementary Figure 8B).

TF distributions affect gene regulation

Because the strength with which bacterial promoters are regulated is a function of the concentration of the relevant transcription factors (Buchler *et al*, 2003; Bintu *et al*, 2005a, b), we next attempt to detect the local enhancement of LacI concentration near the *lacI* gene through the repression strength of a LacI-regulated target. We constructed three families of 14 strains where we inserted into previously

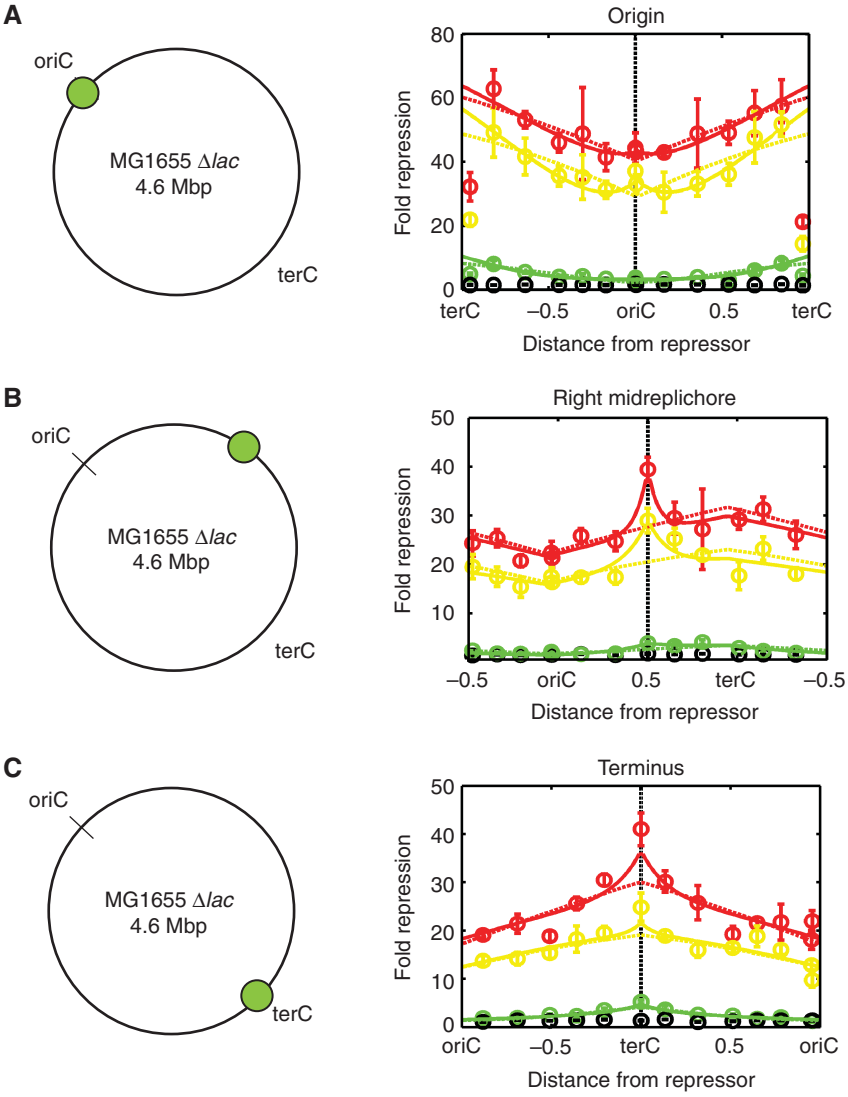

Figure 6 Repression strength as a function of intergenic distance. Repression strength as a function of genomic distance from the *lacI-venus* gene, where *lacI-venus* is near (**A**) origin (*atpI* locus), (**B**) mid-replichore (*ybbD* locus), or (**C**) terminus (*nth* locus). Red: slow growth ($\tau = 110 \pm 12$ min); yellow: medium growth ($\tau = 68 \pm 5$ min); green: fast growth ($\tau = 22 \pm 2$ min); black: M63 + 0.5% glycerol + 2 mM IPTG control; circles are the mean of four measurements, error bars are the s.d. Dashed lines indicate best fits assuming spatially homogeneous distribution of repressor. Solid lines indicate best fits assuming exponential LacI-Venus inhomogeneity. Source data is available for this figure in the Supplementary Information.

constructed *lacI-venus* strains a cassette bearing a LacI-regulated *lacZ* target at regular intervals around the genome (Supplementary Figure 1). In Figure 6A–C, the strength of repression is shown as a function of intergenic distance for each family of strains. Colors indicate the growth rate of the culture: slow (red), medium (yellow); fast (green); slow + 2 mM IPTG control (black). In each plot, the x axis is adjusted so that the location of the repressor gene lies at the center of the x axis (black vertical dashed lines). In all cases, the strength of repression increases as the target is moved toward the terminus and decreases as the target is moved toward the origin. In each case there is a small but reproducible 1.2–2 × spike in repression when the target is located immediately proximal (~200 bp downstream) to the repressor gene. We encounter little interference from position-specific effects, with a few exceptions: in all cases, the target inserted near the terminus at the *essQ* locus (see Supplementary Figure 1) remained unregulated. Additionally, when *lacI-venus* is inserted near the origin (Figure 6A) the repression strengths at *essQ* and *nth* near the terminus are significantly weaker than might otherwise be expected. This may be due to their location within the less densely packed chromosomal crossing region (Wiggins *et al*, 2010). These data were excluded from the best fit lines in Figure 6A–C.

Analysis and modeling: repression strength is inconsistent with a homogeneous TF distribution

To understand these trends, it is necessary to model the response of the reporting promoter to its regulating TF. In steady state, the binding and unbinding of an operator by a TF

is described by the simple equilibrium equation

$$[TF] + [O] \underset{k}{\rightleftarrows} [TF - O]$$
$$K = \frac{[TF][O]}{[TF - O]}. \quad (2)$$

Consequently, at equilibrium any effects of TF-target intergenic spacing can be exerted only through the TF concentration, [TF], the concentration of the target operator, [O], and/or the equilibrium dissociation constant K.

In Equation (2) the operator concentration, [O], changes due to the absolute location of genes relative to the replication origin. Because replication initiation and elongation occur from a single origin in *E. coli*, the period-averaged average gene copy number varies as a function of position according to

$$\langle [\mathrm{O}(x)] \rangle = 2^{[C(1-x)+D]/\tau} \quad (3)$$

where C is the time to complete replication (40–70 min), D is the time lag between completion of replication and cell division (22–30 min), τ is the doubling time of the culture, and x is the fractional location of the gene between the replication origin and terminus (origin at $x = 0$ and terminus at $x = 1$) (Cooper and Helmstetter, 1968; Helmstetter and Cooper, 1968; Bremer and Churchward, 1977; Bremer and Dennis, 1996). Because at the fastest growth rates reinitiation of replication occurs before the first termination, on average there can be as many as eight copies of origin-proximal genes for every one terminus-proximal gene. Increased intergenic spacing therefore leads to an imbalance of relative TF-target gene copy numbers if TF and target genes are located at disparate locations on the chromosome.

To describe the repression data, we combine Equations (2) and (3) with a statistical mechanical model of transcriptional regulation of the promoter expressing *lacZ* (Buchler *et al*, 2003; Bintu *et al*, 2005a, b). For the promoter used in these experiments, we find that the repression strength, ρ, can be predicted as

$$\rho = 1 + \frac{[\mathrm{TF}]}{K} \quad (4)$$

(see Supplementary information—Promoter Modeling and Supplementary Figure 9). This model is used to fit the data in Figure 6.

We first fit the data assuming a spatially homogeneous distribution of repressor (dashed colored lines in Figure 5A–C). The fits recapitulate the general trends: as the target is moved toward the terminus the ratio of average TF to target gene number increases, leading to increased repression strength. Conversely, when the target is moved toward the origin, the ratio of average TF to target gene number decreases, resulting in decreased repression strength.

While these fits display the correct general trends, in all cases the strength of repression near the TF gene is $\sim 1.5\times$ stronger than predicted by the null model. We note the similarity of this enhancement to the observed enhancement of LacI-Venus concentration summarized in Figure 2. According to Equation (4), ρ increases linearly with [TF] for this promoter; therefore, increases in TF concentration should result in corresponding enhancements in repression strength.

Analysis and modeling: repression strength is consistent with local inhomogeneity

Keeping the microscopy results in mind, we next incorporate a local TF concentration gradient into our model. Since we assume that the gradient is generated by diffusion, and a steady-state diffusion gradient with constant linear degradation is exponential regardless of the details of the diffusion process (dimensionality, diffusion versus anomalous diffusion, etc.) (Hornung *et al*, 2005), we postulate a local exponential gradient that decays to a non-zero background concentration of repressor:

$$[\mathrm{TF}(x)] = [\mathrm{TF}][1 + \gamma \exp(-|x - x_0|/\lambda)] \quad (5)$$

where x_0 is the location of the TF gene and x is the location in space where the concentration is being measured. The first term describes a constant background distribution of TF, while the second term describes a local exponential concentration gradient characterized by two additional parameters: a length scale λ and a local enhancement factor γ (we consider the origins of such a function in Discussion).

Combining Equation (5) into our model and fitting the repression strength data yields the solid lines in Figure 6 and the fit parameters in Supplementary Table 2. In contrast to the fits assuming homogeneous repressor concentration, this model recapitulates the trends in the data as well as the local enhancement of repression near the TF gene. Given that $K_{\mathrm{Oid}} \sim 0.1$ nM (Oehler *et al*, 1994, 2006), the extracted TF concentrations are in the range of 0.1–14 nM (Gilbert and Muller-Hill, 1966); the smallest values can possibly be explained as a consequence of increasing K due to growth effects (see Supplementary information—Dilution and Growth Effects and Supplementary Figure 10).

Discussion

The origins of TF inhomogeneity

That steady-state TF concentration inhomogeneity can be observed at all is surprising given the small size of the cell and the time scales involved. In *E. coli*, TFs are produced from a localized source due to the persistent localization of mRNAs observed previously (Montero Llopis *et al*, 2010) and in this report and the spatial coupling of transcription and translation. Naïvely, as repressor diffuses away from this source, the shape of the resulting gradient should be determined by the ratio of the diffusion constant to the degradation rate of the TF (Ibanes and Izpisua Belmonte, 2008). The *in vivo* diffusion constant of LacI-Venus has been measured by live tracking of individual molecules to be $\sim 0.4\ \mu\mathrm{m}^2/\mathrm{s}$ (Elf *et al*, 2007), and the average time required for LacI-Venus to diffuse from one end of the cell to the other is therefore on the order of 1–10 s. The proteolytic degradation rate of LacI, on the other hand, is thought to be sufficiently small that dilution due to growth is generally assumed to be the primary mechanism for depletion (e.g., Narang and Pilyugin, 2008). That the dilution time scale is a minimum of 100–1000$\times$ slower than the diffusion time scale might lead one to expect that significant steady-state intracellular TF concentration inhomogeneity is impossible and that the intracellular TF concentration will rapidly homogenize.

From a physical point of view, the observed inhomogeneity of TFs can be explained only by a limited variety of mechanisms, and all of these mechanisms may be at play to some degree. One possibility is that the system could be heterogeneous as a transient state. This explanation appears to be ruled out as such transient states should be short lived based upon the known rates of diffusion observed by live tracking of individual molecules (Elowitz *et al*, 1999; Elf *et al*, 2007). However, since live tracking requires the maturation of fluorophores before they can be imaged ($\sim$10 min for Venus; Nagai *et al*, 2002; Elf *et al*, 2007), it is possible that there exist intranucleoid states immediately after TF production which diffuse anomalously or more slowly than heretofore reported.

Another possibility is spatial heterogeneity of diffusion coefficients. However, this mechanism can only maintain inhomogeneity if there is localized production of TFs combined with degradation (Ibanes and Izpisua Belmonte, 2008; Wartlick *et al*, 2009). TFs are produced locally as a consequence of the persistent localization of mRNAs at the site of transcription (Montero Llopis *et al*, 2010) and the spatial coupling of transcription and translation. Under these conditions, the steady state resulting from localized production balanced with degradation, dilution, or nucleoid exclusion can lead to TF inhomogeneity within the nucleoid.

Finally, spatial heterogeneity can be driven by spatial variation in energetic potentials for DNA, mRNA, and TFs, resulting in heterogeneity even at thermodynamic equilibrium. These spatial variations are almost certainly important here due to, e.g., the energetic favorability of TF-DNA binding and the observed exclusion of proteins from highly compacted DNA, perhaps driven by entropic mechanisms (Saberi and Emberly, 2010).

We propose that the observed inhomogeneity is the result of competing forces of binding to DNA on one hand and exclusion from DNA on the other hand, and that the relative magnitude of these forces is dependent upon the local DNA compaction density. That the magnitude of the exclusion force is an increasing function of DNA density can be observed straightforwardly by examining the degree of exclusion of LacI42-Venus as a function of growth rate. With fast growth and low DNA density (last column in Figure 4), mutant LacI42-Venus is not obviously excluded from the DNA volume. However, as growth rate decreases and compaction increases, exclusion increases until the mutant LacI42-Venus is more highly localized toward the ends of the cells in stationary phase (second column in Figure 3).

These competing forces will influence the diffusive kinetics of TFs within the nucleoid. In steady state, we propose to describe intranucleoid diffusion by a mean-field model in which TFs can be separated into two sub-populations: those TFs confined within the nucleoid, $[TF_1]$, and those TFs undergoing 3D diffusion in the cytoplasm, $[TF_3]$:

$$\begin{aligned}\frac{\partial[TF_1(\vec{x},t)]}{\partial t} &= \alpha f\delta(\vec{x}-\vec{x}_0) + D_1\nabla^2[TF_1] - (k_1+\beta)[TF_1] + k_2[TF_3]\\ \frac{\partial[TF_3(\vec{x},t)]}{\partial t} &= \alpha(1-f)\delta(\vec{x}-\vec{x}_0) + D_3\nabla^2[TF_3]\\ &\quad - (k_2+\beta)[TF_3] + k_1[TF_1]\end{aligned} \tag{6}$$

where α is the rate of TF production, β is the rate constant for degradation or dilution, D_1 and D_3 are the intranucleoid and extranucleoid diffusion coefficients, respectively, k_1 and k_2 are nucleoid exclusion and capture rate constants, respectively, and f is the fraction of TFs initially confined to the nucleoid after translation. We postulate that hops through 3D space of short duration within the nucleoid can be coarse grained along with true 1D sliding along DNA into effective 1D diffusion along the nucleoid. Only when TFs escape into the cytoplasm for an extended 3D excursion they are considered to be undergoing true 3D diffusion, and this escape is assumed to occur with linear rate constant k_1 as a result of nucleoid exclusion forces. In this view, the escape rate constant k_1 serves as the degradation rate constant of the nucleoid-confined sub-population. After escape, TFs diffusing in 3D rapidly form a homogeneous background pool and can be recaptured by the nucleoid with linear rate constant k_2. A cartoon illustrating this argument is shown in Figure 7. The steady-state solution of a simplified 1D version of this model yields an enhancement of TF concentration around the encoding gene located at a position x_0 (Kuhlman and Cox, in preparation):

$$[TF(x)] = [TF][1+\gamma\ \exp(-\mid x-x_0\mid/\lambda)] \tag{7}$$

where x is the longitudinal distance from the source gene and we define the constants

$$\begin{aligned}[TF] &\equiv \frac{k_2}{k_1}[TF_3], \quad \gamma \equiv \frac{\alpha f}{[TF]\sqrt{D_1(k_1+\beta)}},\\ \lambda &\equiv \sqrt{D_1/(k_1+\beta)}\end{aligned} \tag{8}$$

The solution (7) is precisely the functional form postulated in Equation (5), and has two terms: a constant background concentration [TF], and a local enhancement of concentration around the encoding gene whose magnitude relative to the background is characterized by the parameter γ. This parameter is directly proportional to the fraction of TFs immediately captured by the nucleoid after translation, f. Thus, when the source of production is located within the nucleoid, $f>0$, yielding non-zero γ and localized

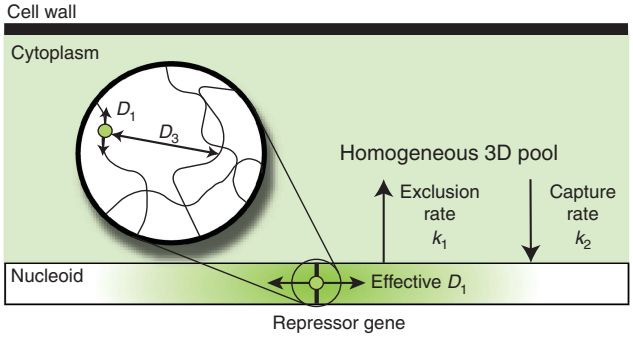

Figure 7 A model of intranucleoid diffusion. TFs are produced at the site of the source gene within the nucleoid. TFs are initially confined to the nucleoid and diffuse via 1D sliding along the chromosome combined with short 3D hops between domains, which we coarse grain together as effective 1D diffusion along the entire nucleoid. TFs are excluded from the nucleoid with rate constant k_1, where they quickly homogenize via rapid 3D diffusion to form a background pool of repressor. TFs can be recaptured into the nucleoid rate constant k_2, and are diluted with rate constant β.

inhomogeneity. When TFs are produced from an extrachromosomal source such as a plasmid directly into the cytoplasm, $f = 0$, and this results in homogeneous distribution throughout the DNA, as observed experimentally (Figure 2).

After production, it takes ~10 min for the Venus fluorophore to mature (Nagai *et al*, 2002; Elf *et al*, 2007), a process that occurs even after fixation by paraformaldehyde (Little *et al*, 2011). Thus, we believe that our results remain consistent with previous live-tracking measurements of rapid intracellular TF diffusion (Elf *et al*, 2007) because live tracking requires the fluorophore to mature before it can be visualized. The nucleoid bound state leading to inhomogeneity, $[TF_1]$, may decay before maturation, and we argue that the cytoplasmic fraction $[TF_3]$, interacting with the nucleoid, may primarily be what was imaged in live-tracking experiments.

The observations reported in this manuscript are in accord with previous reports regarding *cis*-acting proteins, such as the λ-phage Q protein (Echols *et al*, 1976), the bacteriophage φX174 A protein (Francke and Ray, 1972), and the IS10 transposase of the Tn10 system (Morisato *et al*, 1983; Jain and Kleckner, 1993). These proteins have been shown to preferentially act upon closely located targets (Morisato *et al*, 1983; Jain and Kleckner, 1993), or to act only while synthesis is in progress, but cease to function later, even though intact and functional protein is still present (Echols *et al*, 1976). They are also generally DNA binding proteins, and their initial mechanism of action is similar to that of TFs such as LacI: the recognition of, and binding to, some cognate DNA sequence. This binding and unbinding will be governed by an equilibrium analogous to Equation (2), and we therefore suggest that the observed preferential *cis*-action may also be a consequence of protein inhomogeneity and concentration near the source gene. Furthermore, the activity of the IS10 transposase on transposons has been assayed as a function of the transposase/transposon intergenic distance (Morisato *et al*, 1983; Jain and Kleckner, 1993), and from an analysis of this data we find that this activity decays exponentially with distance, similar to that reported here with Lac repressor and modeled in Equations (5) and (7) (see Supplementary Figure 11).

We also expect that the same rules of intranuceloid versus cytoplasmic production should influence the diffusive kinetics and spatial distribution of RNAs, and the results presented here may reconcile the apparent discrepancy between the observation of the rapid diffusion rates of RNAs (Golding and Cox, 2004; Golding *et al*, 2005) contrasted with the apparent colocalization of RNAs with chromosomally located source genes reported here and by Montero Llopis *et al* (2010). The rapid diffusion rates for RNAs observed by Golding and Cox resulted from quantitative measurement of RNAs produced from polar-localized bacterial artificial chromosomes; i.e., the RNAs were transcribed directly into the cytoplasm ($f = 0$, Equation (6)). This is similar to the extrachromosomal plasmid reported here where it appears that the RNAs it produces have an enhanced tendency to redistribute compared with chromosomally produced RNAs (Figure 2; Supplementary Figure 5B). We might also expect that the diffusive kinetics of RNAs transcribed within the nucleoid are significantly different from those transcribed in the cytoplasm, and that the more crowded intranuceloid environment will lead to slower rates of diffusion and a higher degree of RNA/gene colocalization.

Dynamic nucleoid organization as a regulatory strategy

The observation that *E. coli* can dynamically alter the distribution of TFs and other intracellular proteins by changing the compaction state of its DNA may provide a mechanism by which *E. coli* can shift between global gene expression patterns. It has been previously demonstrated that *E. coli* generally reduces the expression of genes near the origin of replication and increases the expression of genes near the terminus upon DNA condensation (Berger *et al*, 2010). We note that since origin proximal genes lie within the body of the nucleoid and terminal-proximal genes lie within the loosely packed chromosomal crossing region which is exposed to the cytoplasm (Wiggins *et al*, 2010), these changes in gene expression correlate with the spatial changes in TF and protein distribution we observe during chromosomal condensation. Furthermore, we also observe reorganization and redistribution of DNA and protein upon exposure to serine hydroxamate, which induces the stringent response via amino-acid starvation (Ferullo and Lovett, 2008; Supplementary Figure 7B). We therefore suggest that protein redistribution driven by DNA condensation may be a general strategy for quickly altering global gene expression patterns in response to environmental stimuli, and, in particular, for sweeping non-specifically bound TFs from the DNA.

Implications for bacterial genome organization

There is mounting evidence that the spatial organization of the prokaryotic genome is determined by the connectivity and co-regulation of transcriptional regulatory networks, rather than through selection via horizontal gene transfer (Pál and Hurst, 2004; Warren and ten Wolde, 2004; Hershberg *et al*, 2005; Price *et al*, 2005; Kolesov *et al*, 2007; Wunderlich and Mirny, 2008; Janga *et al*, 2009; Yin *et al*, 2010). This work provides experimental evidence for a possible mechanism driving this organization. Because of the inhomogeneity of the intracellular TF concentration, gene targets are regulated more strongly and more quickly when located closer to their regulatory TF genes (Kolesov *et al*, 2007; Wunderlich and Mirny, 2008; Mirny *et al*, 2009). Because spatial distance is directly proportional to genomic distance (Wiggins *et al*, 2010), these regulatory benefits may provide selective pressure driving the close genomic organization of co-regulated genes on the bacterial chromosome.

Implications for eukaryotes

Because eukaryotic TF proteins are not produced locally, transcriptional regulation of eukaryotic genes by TFs is not subject to the same effects of TF gene localization in bacteria that we focus upon here. However, the sites of nuclear re-importation serve as localized sources and may result in intranuclear TF inhomogeneity. This naïve preconception may anticipate recent studies that reveal that some regulated genes

in yeast actively reorganize to the nuclear periphery and associate with nuclear pores upon exposure to inducing conditions (Ahmed and Brickner, 2007; Brickner *et al*, 2007; Ahmed *et al*, 2010).

Materials and methods

Strains and plasmids

All strains used in this study are derivatives of *E. coli* K-12 MG1655 Δ*lac* (Kuhlman and Cox, 2010), in which the entire *lac* operon has been deleted from the N-terminus of *lacI* to the C terminus of *lacA* using the method of Datsenko and Wanner (2000). Strains with P_{lacI}-*lacI-venus::T1* (Nagai *et al*, 2002; Elf *et al*, 2007; Kuhlman and Cox, 2010) integrated at specific locations in the chromosome were constructed using Landing Pad technology as described previously (Kuhlman and Cox, 2010) and in Supplementary information. Required permissions for use of *venus* were obtained from Dr Atsushi Miyawaki at the Riken Brain Science Institute.

Media and growth conditions

To obtain various doubling times, cells were grown at 37°C in a shaking water bath with M63 medium (100 mM KH_2PO_4, 15 mM $(NH_4)_2SO_4$, 1.7 μM $FeSO_4$, 1 mM $MgSO_4$) + 0.5% glycerol, or Rich Defined Medium (Teknova) + 0.5% glucose without antibiotics. We estimate that at the time of harvest cells had been growing in exponential steady state for ~10 generations. Representative growth curves for each growth condition are shown in Supplementary Figure 2. A detailed protocol for cell growth can be found in Supplementary Information. For fixation, an equal volume of freshly prepared and filtered 5% paraformaldehyde in phosphate-buffered saline (PBS) was added directly to each culture. The resulting solution was allowed to continue shaking at 37 °C for 10 min and was then placed on ice for 30 min. Cells were washed three times via centrifugation and resuspension in 1 ml filtered, ice-cold PBS.

Fluorescent reporter-operator system

Gene locations were determined using the FROS performed as described in Joshi *et al* (2011), the components of which were the kind gift of David Bates. Integrations were made at each site consisting of an array of 240 operators for *tet* repressor, TetR, using the Landing Pad technology. After growth to steady state as described above, 0.01% L-arabinose was added to each culture 1 h before fixation to induce expression of TetR tagged with fluorescent EYFP in *trans* from the plasmid pBH74 (Joshi *et al*, 2011). Cells were then fixed and processed as above.

Fluorescent *in situ* hybridization

mRNA locations were determined by single-molecule FISH, performed as described in So *et al* (2011) using an array of 48 bp Stellaris FISH probes covering the coding sequence of *lacI* and labeled with CAL Fluor Red 590 purchased from Biosearch Technologies. Control experiments using similarly prepared probes for the coding strand of DNA yielded no bright spots, demonstrating specific labeling of mRNA.

After fixation, cells in PBS were spread onto poly-L-lysine coated #1 22 mm × 60 mm coverslips and allowed to adhere for 30 min. Coverslips were rinsed with PBS and soaked in 70% ethanol for 1 h to permeabilize the cell wall. The slides were then rinsed in wash buffer (40% formamide, 2× SSC buffer). In all, 100 μl of hybridization solution (40% formamide, 2× SSC buffer, 1 mg/ml *E. coli* tRNA, 200 μg/ml BSA, 2 μM ribonucleoside vanadyl complex, 2 μl of 2.5 μM probe stock) was added to each coverslip, which was then covered with two 22 mm × 22 mm HybriSlip hybridization covers (Invitrogen). The coverslips were enclosed in watertight aluminum slide chambers and hybridized overnight in a 30°C water bath. The next morning, slips were washed three times for 30 min each in wash buffer warmed to 30°C. They were then rinsed once in 2× SSC and once in PBS, and finally mounted on glass slides with 40% glycerol.

Microscopy

After the appropriate preparation for the sample, the prepared coverslips were mounted on glass slides using 40% glycerol and, if appropriate, 5 μg/ml DAPI as a DNA stain. Nucleoid, FROS, and mRNA imaging were performed using a Nikon Eclipse TE2000U microscope with an Applied Scientific Instruments PZM-2000 automated stage utilizing Metamorph automation software. Images were gathered using epifluorescent illumination of the appropriate wavelength with a ×100 phase contrast objective combined with a ×4 telescope attachment using a Roper Scientific Cascade:512 camera.

Single-molecule LacI-Venus microscopy was performed using a Nikon Eclipse TE2000U microscope with either a 488-nm laser (10 mW) or a 515-nm laser to improve the signal-to-noise ratio for LacI-Venus when needed, a TIRF microscopy attachment, and a Prior ProScan II automated stage using Andor iXon Basic software at ×133 (for visual clarity in representative images) or ×400 magnification (for image averaging). Emitted light was collected through the appropriate filter (ET 535/30 M) and the image captured by an Andor DV877-DCS-BV electron multiplying charge coupled device (EMCCD) camera. Imaging of the nucleoid with the same TIRF microscope after staining with SYBR green I (Invitrogen) yields the same average DNA distribution as that obtained with epifluorescent illumination of DAPI-stained cells at all growth rates, indicating that the penetration depth of the evanescent TIRF wave is sufficiently deep to observe a volume representative of the entire nucleoid.

Data and image analysis

All data and images were analyzed using custom software written in MATLAB 2010a (MathWorks). The distribution of LacI-Venus in each figure is determined as the difference in average spatial distribution of fluorescence in a LacI-Venus strain minus the average spatial distribution of autofluorescence of the same strain without the *lacI-venus* integration, grown under identical conditions. In particular, distributions obtained after the addition of chloramphenicol in Figure 5 were compared with samples of the negative control treated identically with chloramphenicol at each time point. Image analysis is discussed thoroughly in Supplementary Information—Image Analysis.

LacZ measurements

For measurements of repression strength, the cells were grown as described above, and LacZ activity measured using traditional methods (Miller, 1972). When the density of the culture reached $OD_{600} = 0.2–0.4$, a 0.5-ml sample of culture was added directly to 0.5 ml Z-buffer (Miller, 1972) and 40 μl chloroform (Fisher Scientific). Each sample was thoroughly mixed via repeated pipetting. In all, 200 μl of 4 mg/ml ortho-nitrophenyl-β-galactoside (ONPG; Sigma-Aldrich) in Z-buffer was added. When sufficient yellow color had developed to be visible by eye, 500 μl of 1 M Na_2CO_3 was added and the elapsed time recorded. OD_{420} and OD_{550} of each sample were measured in a spectrophotometer (Bio-Rad SmartSpec 3000) and the LacZ activity, α, was calculated as

$$\alpha = 1000 \times \frac{\mathrm{OD420} - 1.75 \times \mathrm{OD550}}{2 \times \Delta t \times \mathrm{OD600}} \tag{9}$$

Repression strength, ρ, defined as

$$\rho = \alpha_- / \alpha_+ \tag{10}$$

and shown in Figure 6 is the ratio of the average of four measurements from independent cultures of each strain with (α_+) or without (α_-) *lac* repressor. Error bars are calculated as

$$\sigma_\rho = \langle \rho \rangle \times \sqrt{\sum_{i=+/-} \left(\frac{\sigma_{\alpha_i}}{\langle \alpha_i \rangle} \right)^2} \tag{11}$$

where σ_{α_i} are the standard deviations of the four measurements of α_+ and α_-.

Supplementary information

Supplementary information is available at the *Molecular Systems Biology* website (www.nature.com/msb).

Acknowledgements

We would like to thank Drs Sunney Xie and Atsushi Miyawaki for providing Venus constructs and the required permissions for their use; Dr David Bates for providing materials for FROS; and Drs Stephan Thiberge, Phuon Ong, and Bob Austin for assistance with microscopy. We would like to thank Justin Kinney, Simon Nørrelykke, Robert Cooper, Rob Phillips, Hernan Garcia, Terry Hwa, Ido Golding, Matthew Scott, Ned Wingreen, and Leonid Mirny for thoughtful discussions. This work was supported by the National Institutes of Health (GM078591, GM071508) and the Howard Hughes Medical Institute (52005884). TEK is supported by an NIH Ruth Kirschstein NRSA Fellowship (F32GM090568-01A1).

Author contributions: TEK and ECC designed experiments and wrote the paper. TEK performed all strain construction, experiments, modeling and analysis.

Conflict of interest

The authors declare that they have no conflict of interest.

References

Ahmed S, Brickner DG, Light WH, Cajigas I, McDonough M, Froyshteter AB, Volpe T, Brickner JH (2010) DNA zip codes control an ancient mechanism for gene targeting to the nuclear periphery. *Nat Cell Biol* **12:** 111–118

Ahmed S, Brickner JH (2007) Regulation and epigenetic control of transcription at the nuclear periphery. *Trends Genet* **23:** 396–402

Bates D, Kleckner N (2005) Chromosome and replisome dynamics in E. coli: loss of sister cohesion triggers global chromosome movement and mediates chromosome segregation. *Cell* **121:** 899–911

Berg OG, Winter RB, von Hippel PH (1981) Diffusion-driven mechanisms of protein translocation on nucleic acids. 1. Models and theory. *Biochemistry* **20:** 6929–6948

Berger M, Farcas A, Geertz M, Zhelyazkova P, Brix K, Travers A, Muskhelishvili G (2010) Coordination of genomic structure and transcription by the main bacterial nucleoid-associated protein HU. *EMBO Rep* **11:** 59–64

Bintu L, Buchler NE, Garcia HG, Gerland U, Hwa T, Kondev J, Kuhlman T, Phillips R (2005a) Transcriptional regulation by the numbers: applications. *Curr Opin Genet Dev* **15:** 125–135

Bintu L, Buchler NE, Garcia HG, Gerland U, Hwa T, Kondev J, Phillips R (2005b) Transcriptional regulation by the numbers: models. *Curr Opin Genet Dev* **15:** 116–124

Bremer H, Churchward G (1977) An examination of the Cooper-Helmstetter theory of DNA replication in bacteria and its underlying assumptions. *J Theor Biol* **69:** 645–654

Bremer H, Dennis PP (1996) Modulation of chemical composition and other parameters of the cell by growth rate. In *Escherichia coli and Salmonella: Cellular and Molecular Biology*, Neidhardt FC (ed) Vol. 22, 5th edn, pp 1553–1569. Washington, DC: ASM Press.

Brickner DG, Cajigas I, Fondufe-Mittendorf Y, Ahmed S, Lee PC, Widom J, Brickner JH (2007) H2A.Z-mediated localization of genes at the nuclear periphery confers epigenetic memory of previous transcriptional state. *PLoS Biol* **5:** e81

Buchler NE, Gerland U, Hwa T (2003) On schemes of combinatorial transcription logic. *Proc Natl Acad Sci USA* **100:** 5136–5141

Cabrera JE, Cagliero C, Quan S, Squires CL, Jin DJ (2009) Active transcription of rRNA operons condenses the nucleoid in Escherichia coli: examining the effect of transcription on nucleoid structure in the absence of transertion. *J Bacteriol* **191:** 4180–4185

Cooper S, Helmstetter CE (1968) Chromosome replication and the division cycle of Escherichia coli B/r. *J Mol Biol* **31:** 519–540

Datsenko KA, Wanner BL (2000) One-step inactivation of chromosomal genes in Escherichia coli K-12 using PCR products. *Proc Natl Acad Sci USA* **97:** 6640–6645

Ebersbach G, Briegel A, Jensen GJ, Jacobs-Wagner C (2008) A self-associating protein critical for chromosome attachment, division, and polar organization in Caulobacter. *Cell* **134:** 956–968

Echols H, Court D, Green L (1976) On the nature of cis-acting regulatory proteins and genetic organization in bacteriophage: the example of gene Q of bacteriophage lambda. *Genetics* **83:** 5–10

Elf J, Li GW, Xie XS (2007) Probing transcription factor dynamics at the single-molecule level in a living cell. *Science* **316:** 1191–1194

Elowitz MB, Surette MG, Wolf PE, Stock JB, Leibler S (1999) Protein mobility in the cytoplasm of Escherichia coli. *J Bacteriol* **181:** 197–203

Ferullo DJ, Lovett ST (2008) The stringent response and cell cycle arrest in *Escherichia coli*. *PLoS Genet* **4:** e1000300

Francke B, Ray DS (1972) Cis-limited action of the gene-A product of bacteriophage phiX174 and the essential bacterial site (E. coli-electron microscopy-cis-acting protein-specifically-nicked RF). *Proc Natl Acad Sci USA* **69:** 475–479

Gerland U, Moroz JD, Hwa T (2002) Physical constraints and functional characteristics of transcription factor-DNA interaction. *Proc Natl Acad Sci USA* **99:** 12015–12020

Gilbert W, Muller-Hill B (1966) Isolation of the lac repressor. *Proc Natl Acad Sci USA* **56:** 1891–1898

Golding I, Cox EC (2004) RNA dynamics in live Escherichia coli cells. *Proc Natl Acad Sci USA* **101:** 11310–11315

Golding I, Paulsson J, Zawilski SM, Cox EC (2005) Real-time kinetics of gene activity in individual bacteria. *Cell* **123:** 1025–1036

Helmstetter CE, Cooper S (1968) DNA synthesis during the division cycle of rapidly growing Escherichia coli B/r. *J Mol Biol* **31:** 507–518

Hershberg R, Yeger-Lotem E, Margalit H (2005) Chromosomal organization is shaped by the transcription regulatory network. *Trends Genet* **21:** 138–142

Hornung G, Berkowitz B, Barkai N (2005) Morphogen gradient formation in a complex environment: An anomalous diffusion model. *Phys Rev E* **72:** 041916

Ibanes M, Izpisua Belmonte JC (2008) Theoretical and experimental approaches to understand morphogen gradients. *Mol Syst Biol* **4:** 176

Jain C, Kleckner N (1993) Preferential cis action of IS 10 transposase depends upon its mode of synthesis. *Mol Microbiol* **9:** 249–260

Janga SC, Salgado H, Martinez-Antonio A (2009) Transcriptional regulation shapes the organization of genes on bacterial chromosomes. *Nucleic Acids Res* **37:** 3680–3688

Joshi MC, Bourniquel A, Fisher J, Ho BT, Magnan D, Kleckner N, Bates D (2011) Escherichia coli sister chromosome separation includes an abrupt global transition with concomitant release of late-splitting intersister snaps. *Proc Natl Acad Sci USA* **108:** 2765–2770

Kolesov G, Wunderlich Z, Laikova ON, Gelfand MS, Mirny LA (2007) How gene order is influenced by the biophysics of transcription regulation. *Proc Natl Acad Sci USA* **104:** 13948–13953

Kubitschek HE (1974) Constancy of the ratio of DNA to cell volume in steady-state cultures of Escherichia coli B-r. *Biophys J* **14:** 119–123

Kuhlman TE, Cox EC (2010) Site-specific chromosomal integration of large synthetic constructs. *Nucleic Acids Res* **38:** e92

Little SC, Tkačik G, Kneeland TB, Wieschaus EF, Gregor T (2011) The formation of the bicoid morphogen gradient requires protein movement from anteriorly localized mRNA. *PLoS Biol* **9:** e1000596

Lutz R, Bujard H (1997) Independent and tight regulation of transcriptional units in Escherichia coli via the LacR/O, the TetR/O and AraC/I1-I2 regulatory elements. *Nucleic Acids Res* **25:** 1203–1210

Miller JH (1972) *Experiments in Molecular Genetics*. Plainview, NY: Cold Spring Harbor Press
Mirny L *et al* (2009) How a protein searches for its site on DNA: the mechanism of facilitated diffusion. *J Phys A: Math Theor* **42:** 434013
Montero Llopis P, Jackson AF, Sliusarenko O, Surovtsev I, Heinritz J, Emonet T, Jacobs-Wagner C (2010) Spatial organization of the flow of genetic information in bacteria. *Nature* **466:** 77–81
Morisato D, Way JC, Kim H-J, Kleckner N (1983) Tn10 transposase acts preferentially on nearby transposon ends *in vivo*. *Cell* **32:** 799–807
Müller-Hill B (1998) The function of auxiliary operators. *Mol Microbiol* **29:** 13–18
Nagai T, Ibata K, Park ES, Kubota M, Mikoshiba K, Miyawaki A (2002) A variant of yellow fluorescent protein with fast and efficient maturation for cell-biological applications. *Nat Biotechnol* **20:** 87–90
Narang A, Pilyugin SS (2008) Bistability of the lac operon during growth of Escherichia coli on lactose and lactose + glucose. *Bull Math Biol* **70:** 1032–1064
Niki H, Yamaichi Y, Hiraga S (2000) Dynamic organization of chromosomal DNA in Escherichia coli. *Genes Dev* **14:** 212–223
Oehler S, Alberti S, Müller-Hill B (2006) Induction of the lac promoter in the absence of DNA loops and the stoichiometry of induction. *Nucleic Acids Res* **34:** 606–612
Oehler S, Amouyal M, Kolkhof P, von Wilcken-Bergmann B, Muller-Hill B (1994) Quality and position of the three lac operators of E. coli define efficiency of repression. *EMBO J* **13:** 3348–3355
Oehler S, Eismann ER, Kramer H, Muller-Hill B (1990) The three operators of the lac operon cooperate in repression. *EMBO J* **9:** 973–979
Pál C, Hurst LD (2004) Evidence against the selfish operon theory. *Trends Genet* **20:** 232–234
Price MN, Huang KH, Arkin AP, Alm EJ (2005) Operon formation is driven by co-regulation and not by horizontal gene transfer. *Genome Res* **15:** 809–819
Raj A, van den Bogaard P, Rifkin SA, van Oudenaarden A, Tyagi S (2008) Imaging individual mRNA molecules using multiple singly labeled probes. *Nat Methods* **5:** 877–879
Rang Camilla U, Peng Annie Y, Chao L (2011) Temporal dynamics of bacterial aging and rejuvenation. *Curr Biol* **21:** 1813–1816
Saberi S, Emberly E (2010) Chromosome driven spatial patterning of proteins in bacteria. *PLoS Comput Biol* **6:** e1000986
So LH, Ghosh A, Zong C, Sepulveda LA, Segev R, Golding I (2011) General properties of transcriptional time series in Escherichia coli. *Nat Genet* **43:** 554–560
Wang X, Liu X, Possoz C, Sherratt DJ (2006) The two Escherichia coli chromosome arms locate to separate cell halves. *Genes Dev* **20:** 1727–1731
Warren PB, ten Wolde PR (2004) Statistical analysis of the spatial distribution of operons in the transcriptional regulation network of Escherichia coli. *J Mol Biol* **342:** 1379–1390
Wartlick O, Kicheva A, González-Gaitán M (2009) Morphogen Gradient Formation. *Cold Spring Harb Perspect Biol* **1:** a001255
Wiggins PA, Cheveralls KC, Martin JS, Lintner R, Kondev J (2010) Strong intranucleoid interactions organize the Escherichia coli chromosome into a nucleoid filament. *Proc Natl Acad Sci USA* **107:** 4991–4995
Winkler J, Seybert A, Konig L, Pruggnaller S, Haselmann U, Sourjik V, Weiss M, Frangakis AS, Mogk A, Bukau B (2010) Quantitative and spatio-temporal features of protein aggregation in Escherichia coli and consequences on protein quality control and cellular ageing. *EMBO J* **29:** 910–923
Winter RB, Berg OG, von Hippel PH (1981) Diffusion-driven mechanisms of protein translocation on nucleic acids. 3. The Escherichia coli lac repressor—operator interaction: kinetic measurements and conclusions. *Biochemistry* **20:** 6961–6977
Winter RB, von Hippel PH (1981) Diffusion-driven mechanisms of protein translocation on nucleic acids. 2. The Escherichia coli repressor–operator interaction: equilibrium measurements. *Biochemistry* **20:** 6948–6960
Wunderlich Z, Mirny LA (2008) Spatial effects on the speed and reliability of protein-DNA search. *Nucleic Acids Res* **36:** 3570–3578
Yin Y, Zhang H, Olman V, Xu Y (2010) Genomic arrangement of bacterial operons is constrained by biological pathways encoded in the genome. *Proc Natl Acad Sci* **107:** 6310–6315